Low Upper Limit to Methane Abundance on Mars

Christopher R. Webster *et al.*

Science **342**, 355 (2013);
DOI: 10.1126/science.1242902

Low Upper Limit to Methane Abundance on Mars

Christopher R. Webster,[1]* Paul R. Mahaffy,[2] Sushil K. Atreya,[3] Gregory J. Flesch,[1] Kenneth A. Farley,[4] MSL Science Team†

By analogy with Earth, methane in the Martian atmosphere is a potential signature of ongoing or past biological activity. During the past decade, Earth-based telescopic observations reported "plumes" of methane of tens of parts per billion by volume (ppbv), and those from Mars orbit showed localized patches, prompting speculation of sources from subsurface bacteria or nonbiological sources. From in situ measurements made with the Tunable Laser Spectrometer (TLS) on Curiosity using a distinctive spectral pattern specific to methane, we report no detection of atmospheric methane with a measured value of 0.18 ± 0.67 ppbv corresponding to an upper limit of only 1.3 ppbv (95% confidence level), which reduces the probability of current methanogenic microbial activity on Mars and limits the recent contribution from extraplanetary and geologic sources.

Methane is the most abundant hydrocarbon in our solar system and is found in the atmospheres of several planets and satellites (*1*). On Earth, 90 to 95% of atmospheric methane is biologically produced, either from extant or fossil sources, and it is easy to identify and quantify with confidence by using spectroscopic methods (*2*). For Mars, three possible origins have been proposed: geologic, biotic, and exogenous (*3*–*5*). Over the past decade, there have been several reports of methane detection from Earth and from Mars orbit. Observations with the Canada-France-Hawaii Telescope (CFHT) found a global average value of 10 ± 3 parts per billion by volume (ppbv) (*5*). The Planetary Fourier Spectrometer (PFS) on the Mars Express (MEX) spacecraft found a global average abundance of 10 ± 5 ppbv (*4*), later updated (*6*) to 15 ppbv, with indications of discrete localized sources (*4*) and a summer time maximum of 45 ppbv in the north polar region. A search for methane from the Infrared Telescope Facility (IRTF) and the Keck-2 telescope reported methane release in plumes (*7*) from discrete sources in Terra Sabae, Nili Fossae, and Syrtis Major, with the largest plume containing 19,000 tons of CH_4 in March 2003; seasonal changes with a summer time maximum of ~45 ppbv near the equator were seen. Methane abundances later retrieved (*8*) from a second instrument in Mars orbit, the Thermal Emission Spectrometer (TES) of the Mars Global Surveyor (MGS), reported methane abundances as intermittently present (1999 to 2003), ranging from 5 to 60 ppbv in locations where favorable geological conditions such as residual geothermal activity (Tharsis and Elysium) and strong hydration (Arabia Terrae) are expected. More recent observations report methane mixing ratios that have diminished considerably since 2004 to 2006 to upper limits of 7 to 8 ppbv (*9*–*11*), suggesting a very short lifetime for atmospheric CH_4 and contradicting the MEX claim that methane persisted from 2004 to 2010. Ground-based observations favor episodic injection of methane in 1999 and 2003, 10 ppbv at Valles Marineris in February 2006 (*9*, *11*), and <8 ppbv in January 2006 (*10*), 2009, and 2010; whereas orbital data from PFS and TES suggest a more regular behavior with latitudinal, seasonal, and interannual variabilities. At Curiosity's Gale Crater landing site (4.5°S, 137°E), published maps of PFS data (*6*) show an increase from ~15 ppbv in fall to ~30 ppbv in winter, whereas the TES trend (*8*) is opposite: ~30 ppbv in fall and ~5 ppbv in winter.

The Tunable Laser Spectrometer (TLS) of the Sample Analysis at Mars (SAM) (*12*, *13*) instrument suite on the Curiosity rover has a spectral resolution—0.0002 cm^{-1}, which is far superior to those of the ground-based telescopic and orbiting spectrometers—that offers unambiguous identification of methane in a distinct fingerprint spectral pattern of three well-resolved adjacent $^{12}CH_4$ lines in the 3.3 μm band (Fig. 1). The in situ technique of tunable laser absorption in a closed sample cell is simple, noninvasive, and sensitive. TLS is a two-channel tunable laser spectrometer that uses both direct and second harmonic detection of infrared (IR) laser light. One laser source is a near-IR tunable diode laser at 2.78 μm that can scan two spectral regions containing CO_2 and H_2O isotopic lines that have been used to report $^{13}C/^{12}C$, $^{18}O/^{17}O/^{16}O$, and D/H ratios in the Martian atmosphere (*13*). The second laser source is an interband cascade (IC) laser at 3.27 μm used for methane detection alone, scanning across seven rotational lines that includes the R(3) triplet used in this study (Fig. 1 and table S1). The IC laser beam makes 81 passes of a 20-cm-long sample cell of the Herriott design fitted with high-vacuum microvalves that allow evacuation with a turbomolecular pump for "empty cell" scans or filled to Mars ambient pressure (~8 mbar) for "full cell" runs. During data collection, the cell and other optics are kept at 47 ± 3°C by using a heater that thermally stabilizes the cell but is ramped up and down within these temperature limits in order to increase gas sensitivity by spoiling the accumulation of optical interference fringes during the 2-min period of spectrum collection. Our methane determination is made by comparing the measured methane abundances in our sample cell when filled with Mars atmosphere with those of the same cell evacuated, as detailed in (*14*). The laser scans every second through the methane spectral region, and each spectrum is co-added on board to downlink sequential 2-min-averaged spectra during a given run of ~1 to 2 hours in duration. Typically, we recorded 26 2-min "empty cell" spectra followed by 26 2-min "full cell" spectra, then finally five additional 2-min empty cell spectra. For each 2-min spectrum, we retrieved methane abundances from three spectral lines (*14*) individually and combined the results so as to produce a weighted average value. By subtracting all retrieved abundances (full and empty cell) from the empty cell mean value for that sol (one Martian solar day) run, we were left with 31 differences for the empty cell and 26 for the full cell. For our statistical analysis, we analyzed the empty cell and full cell differences for all the sols taken as one data set (*14*). For sols 79, 81, 106, and 292, the foreoptics chamber contained residual terrestrial air (Table 1, pressures), including CH_4, that produced absorption line signals in the sample cell detector channel, as described in (*14*). For sols 306 and 313, the foreoptics was evacuated. Both the sample cell and foreoptics chamber have pressure and temperature sensors. This experiment has been repeated on six separate Martian sols to date (Martian sols 79, 81, 106, 292, 306, and 313 after landing in August 2012). The inlet to the TLS is a stainless steel tube (*14*) heated to 50°C and located on the rover side ~1 m above the Martian surface and was pointed at a variety of directions relative to the nominal wind direction. Mars atmospheric gas was ingested during the night for sols 79, 81, 106, 292, and 313 and during the day for sol 306 (Table 1). Our measurements correspond to southern spring (sols 79, 81, and 106) and mid-late summer (sols 292, 306, and 313) on Mars.

To date, we have no detection of methane. Individually (Table 1), each of our six data sets produces a mean methane value ranging from –2.2 to 1.7 ppbv. Combining the individual sol results with equal weighting yields a mean and SE of 0.11 ± 0.67 ppbv. Alternatively, combining all of the individual measurements from all sols yields a grand mean and SE of 0.18 ± 0.67 ppbv. At the 95% confidence level, either approach (*14*) yields an upper limit on Mars atmospheric methane of 1.3 ppbv. Curiosity's low upper limit is not expected given observations only a few years ago of large methane plumes and calculations (*7*) that the plume dispersion should produce global values of ~6 ppbv after the 6-month period (*3*, *15*) needed to mix uniformly across the planet, which would persist with a photochemical lifetime of several hundred years (*3*, *5*, *16*).

Before Curiosity's landing on Mars in August 2012, observational evidence for methane on

[1]Jet Propulsion Laboratory, California Institute of Technology, Pasadena, CA 91109, USA. [2]NASA Goddard Space Flight Center, Greenbelt, MD 20771, USA. [3]Department of Atmospheric, Oceanic, and Space Sciences, University of Michigan, Ann Arbor, MI 48109, USA. [4]Department of Geological and Planetary Sciences, California Institute of Technology, Pasadena, CA 91125, USA.

*Corresponding author. E-mail: chris.r.webster@jpl.nasa.gov
†MSL Science Team authors and affiliations are listed in the supplementary materials.

Mars was questioned in the published literature (*15*, *17*, *18*). Contradictions were noted between the locations of maxima reported from ground-based observations and maps inferred by PFS and TES from Mars orbit. The plume results (*7*) were questioned (*17*) on the basis of a possible misinterpretation from methane lines whose positions coincided with those of terrestrial isotopic $^{13}CH_4$ lines. Krasnopolsky (*19*) argued that cometary and volcanic contributions were not sufficient to explain high methane abundances, calculating a cometary contribution of only ~0.1 ppbv and noting the lack of current volcanism, lack of hot spots in thermal imaging (*20*), and the extremely low upper limit for Mars SO_2 (*9*, *21*) that in Earth's volcanic emissions is orders of magnitude more abundant than CH_4 (*5*).

The very short methane lifetime of 0.4 to 4 years derived from the 2003–2006 observations (*7*) requires powerful destruction mechanisms that have not been identified to date. Although models have been proposed for rapid removal of methane by oxidants—such as hydrogen peroxide and perchlorates, or by superoxides derived from their mineral reactions (*22*–*24*) and directly by electric fields generated in dust devils (*25*)—there remains no evidence for their existence at Mars. Moreover, it has not been demonstrated that any of these processes can reduce the lifetime of methane by the required factor of 100 or more compared with its photochemical lifetime. Our reported upper limit of 1.3 ppbv is substantially lower than the methane abundances reported from Mars remote sensing spacecraft observations and those from Earth telescopic observations, including both the earlier high values of typically tens of ppbv and the more recently reported upper limits of 7 to 8 ppbv (*9*, *10*). Although TLS samples only the very lowest part (~1 m) of the Mars atmosphere as compared with those of the other observations that are vertical column-integrated results, the atmospheric scale height (~10 km) and mixing

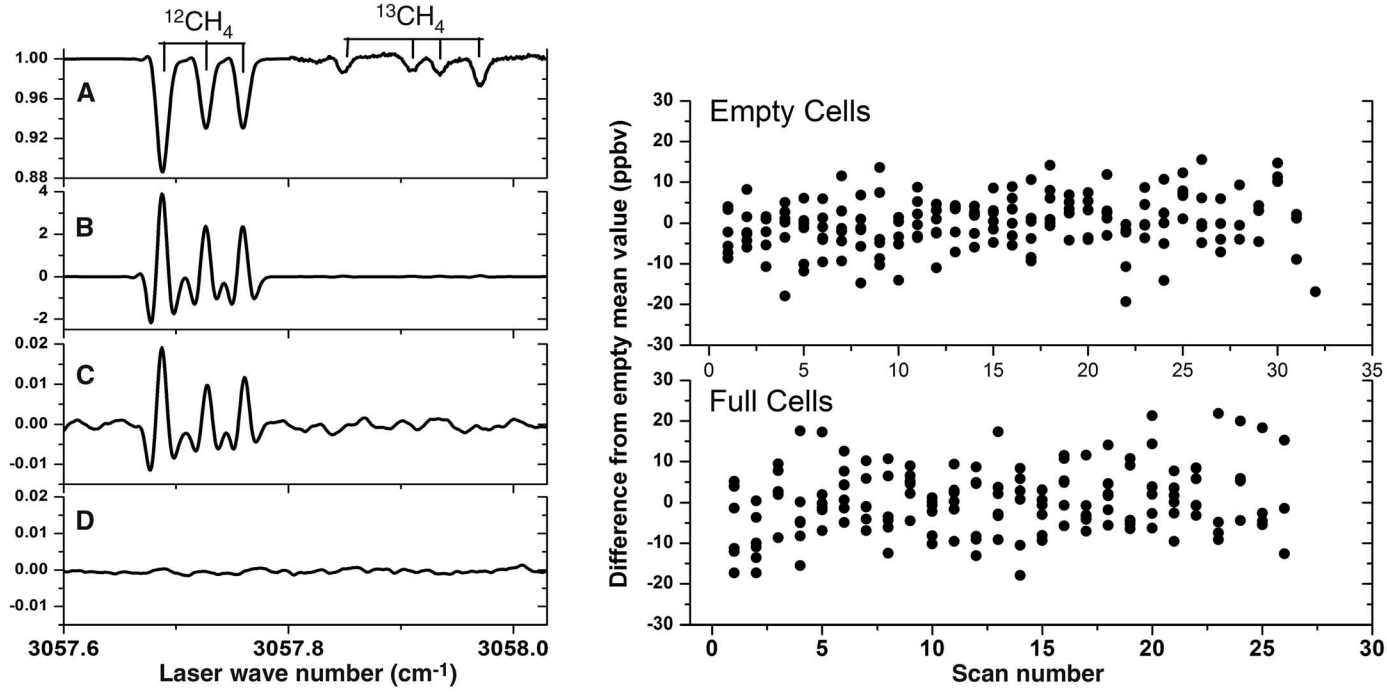

Fig. 1. The TLS-SAM methane measurements. (**Left**) Examples of flight spectra downloaded from Curiosity. (**A**) Spectrum recorded during an unrelated Evolved Gas Analysis (EGA) run (*14*) showing location of $^{12}CH_4$ and $^{13}CH_4$ lines, in which the second half has been vertically expanded by ×20 to show the weaker $^{13}CH_4$ lines. (**B**) Same as (A) but second harmonic (2f) spectrum (*14*), without vertical expansion. (**C**) Averaged full cell 2f spectrum for sol 106 (nighttime ingest), with foreoptics contribution (*14*). (**D**) Averaged full cell 2f spectrum for sol 306 (daytime ingest), with foreoptics evacuated. [Spectra (A) and (B) are shown here in part because they were taken after the atmospheric runs and show that our CH_4 lines have not moved and that the instrument continued to work well with consistent capability to detect methane.] (**Right**) Individual 2-min data points from 6 sols. (Top) Empty cell data with mean value of 0.0 ppbv. (Bottom) Full cell data with mean value of 0.18 ppbv.

Table 1. Curiosity SAM-TLS methane measurements at Gale Crater (4.5°S, 137.4°E) over an 8-month period. SEM, standard error from the mean; Ls, solar longitude.

Martian sol after landing on 6 August 2012	Earth date	Ls (degrees)	Gas ingest time/cell pressure (mbar)/foreoptics pressure (mbar)	Mean value ± 1 SEM (ppbv)
79	25 October 2012	195.0	Night/8.0/11.5	1.62 ± 2.03
81	27 October 2012	196.2	Night/8.0/11.5	1.71 ± 2.06
106	27 November 2012	214.9	Night/8.5/10.9	–0.55 ± 1.45
292	1 June 2013	328.6	Night/8.7/9.2	0.60 ± 1.74
306	16 June 2013	336.5	Day/8.1/0.0	–2.21 ± 0.94
313	23 June 2013	340.5	Night/8.7/0.0	–0.50 ± 0.94
Mean of individual sol results	0.11 ± 0.56			
Mean for entire aggregated data set	0.18 ± 0.67			

time (approximately a few months) suggests that our measured upper limit is representative of the global mean background level. With an expected photochemical lifetime of methane in the Martian atmosphere of hundreds of years (*3*, *5*, *16*), there currently remains no accepted explanation (*15*, *17*) for the existence and distribution of the reported plumes nor of the apparent disappearance of methane over the past few years. Our result sets an upper limit that is ~6 times lower than other recent measurements and greatly reduces the probability of substantial methanogenic microbial activity on Mars and recent methane production through serpentinization or from exogenous sources, including meteoritic, interplanetary dust and cometary infall.

References and Notes

1. S. K. Atreya, P. R. Mahaffy, H. B. Niemann, M. H. Wong, T. C. Owen, *Planet. Space Sci.* **51**, 105–112 (2003).
2. H. A. Michelsen *et al.*, *Geophys. Res. Lett.* **26**, 291–294 (1999).
3. V. A. Krasnopolsky, J. P. Maillard, T. C. Owen, *Icarus* **172**, 537–547 (2004).
4. V. Formisano, S. K. Atreya, T. Encrenaz, N. Ignatiev, M. Giuranna, *Science* **306**, 1758–1761 (2004).
5. S. K. Atreya, P. R. Mahaffy, A. S. Wong, *Planet. Space Sci.* **55**, 358–369 (2007).
6. A. Geminale, V. Formisano, G. Sindoni, *Planet. Space Sci.* **59**, 137–148 (2011).
7. M. J. Mumma *et al.*, *Science* **323**, 1041–1045 (2009).
8. S. Fonti, G. A. Marzo, *Astron. Astrophys.* **512**, A51 (2010).
9. V. A. Krasnopolsky, *Icarus* **217**, 144–152 (2012).
10. G. L. Villanueva *et al.*, *Icarus* **223**, 11–27 (2013).
11. V. A. Krasnopolsky, *EPSC Abstracts* **6**, 49 (2011).
12. P. R. Mahaffy *et al.*, *Space Sci. Rev.* **170**, 401–478 (2012).
13. C. R. Webster *et al.*, MSL Science Team, *Science* **341**, 260–263 (2013).
14. Materials and methods are available as supplementary materials on *Science* Online.
15. F. Lefèvre, F. Forget, *Nature* **460**, 720–723 (2009).
16. A. S. Wong, S. K. Atreya, T. Encrenaz, *J. Geophys. Res.* **108**, (E4), 5026 (2003).
17. K. J. Zahnle, R. S. Freedman, D. C. Catling, *Icarus* **212**, 493–503 (2011).
18. R. A. Kerr, *Science* **338**, 733 (2012).
19. V. A. Krasnopolsky, *Icarus* **180**, 359–367 (2006).
20. P. R. Christensen, *EOS Trans. AGU Fall Meet. Suppl.* **84** (46), Abstract P21A-02, 2003.
21. T. Encrenaz *et al.*, *Astron. Astrophys.* **530**, 1–5 (2011).
22. S. K. Atreya *et al.*, *Planet. Space Sci.* **59**, 133–136 (2011).
23. S. K. Atreya *et al.*, *Astrobiology* **6**, 439–450 (2006).
24. G. T. Delory *et al.*, *Astrobiology* **6**, 451–462 (2006).
25. W. M. Farrell, G. T. Delory, S. K. Atreya, *J. Geophys. Res.* **33**, (2006).

Acknowledgments: The research described here was carried out in part at the Jet Propulsion Laboratory, California Institute of Technology, under a contract with the National Aeronautics and Space Administration (NASA). Data described in the paper are further described in the supplementary materials and have been submitted to NASA's Planetary Data System under an arrangement with the Mars Science Laboratory project.

Supplementary Materials

www.sciencemag.org/content/342/6156/355/suppl/DC1
Materials and Methods
Figs. S1 to S5
Tables S1 to S3
MSL Science Team Author List
References (*26*, *27*)

8 July 2013; accepted 5 September 2013
Published online 19 September 2013;
10.1126/science.1242902

Genomically Recoded Organisms Expand Biological Functions

Marc J. Lajoie,[1,2] Alexis J. Rovner,[3,4] Daniel B. Goodman,[1,5] Hans-Rudolf Aerni,[4,6] Adrian D. Haimovich,[3,4] Gleb Kuznetsov,[1] Jaron A. Mercer,[7] Harris H. Wang,[8] Peter A. Carr,[9] Joshua A. Mosberg,[1,2] Nadin Rohland,[1] Peter G. Schultz,[10] Joseph M. Jacobson,[11,12] Jesse Rinehart,[4,6] George M. Church,[1,13]* Farren J. Isaacs[3,4]*

We describe the construction and characterization of a genomically recoded organism (GRO). We replaced all known UAG stop codons in *Escherichia coli* MG1655 with synonymous UAA codons, which permitted the deletion of release factor 1 and reassignment of UAG translation function. This GRO exhibited improved properties for incorporation of nonstandard amino acids that expand the chemical diversity of proteins in vivo. The GRO also exhibited increased resistance to T7 bacteriophage, demonstrating that new genetic codes could enable increased viral resistance.

The conservation of the genetic code permits organisms to share beneficial traits through horizontal gene transfer (*1*) and enables the accurate expression of heterologous genes in nonnative organisms (*2*). However, the common genetic code also allows viruses to hijack host translation machinery (*3*) and compromise cell viability. Additionally, genetically modified organisms (GMOs) can release functional DNA into the environment (*4*). Virus resistance (*5*) and biosafety (*6*) are among today's major unsolved problems in biotechnology, and no general strategy exists to create genetically isolated or virus-resistant organisms. Furthermore, biotechnology has been limited by the 20 amino acids of the canonical genetic code, which use all 64 possible triplet codons, limiting efforts to expand the chemical properties of proteins by means of nonstandard amino acids (NSAAs) (*7*, *8*).

Changing the genetic code could solve these challenges and reveal new principles that explain how genetic information is conserved, encoded, and exchanged (fig. S1). We propose that genomically recoded organisms (GROs, whose codons have been reassigned to create an alternate genetic code) would be genetically isolated from natural organisms and viruses, as horizontally transferred genes would be mistranslated, producing nonfunctional proteins. Furthermore, GROs could provide dedicated codons to improve the purity and yield of NSAA-containing proteins, enabling robust and sustained incorporation of more than 20 amino acids as part of the genetic code.

We constructed a GRO in which all instances of the UAG codon have been removed, permitting the deletion of release factor 1 (RF1; terminates translation at UAG and UAA) and, hence, eliminating translational termination at UAG codons. This GRO allows us to reintroduce UAG codons, along with orthogonal translation machinery [i.e., aminoacyl–tRNA synthetases (aaRSs) and tRNAs] (*7*, *9*), to permit efficient and site-specific incorporation of NSAAs into proteins (Fig. 1). That is, UAG has been transformed from a nonsense codon (terminates translation) to a sense codon (incorporates amino acid of choice), provided the appropriate translation machinery is present. We selected UAG as our first target for genome-wide codon reassignment because UAG is the rarest codon in *Escherichia coli* MG1655 (321 known instances), prior studies (*7*, *10*) demonstrated the feasibility of amino acid incorporation at UAG, and a rich collection of translation machinery capable of incorporating NSAAs has been developed for UAG (*7*).

We used an in vivo genome-editing approach (*11*), which is more efficient than de novo genome synthesis at exploring new genotypic landscapes and overcoming genome design flaws. Although a single lethal mutation can prevent transplantation of a synthetic genome (*12*), our approach allowed us to harness genetic diversity and evolution to overcome any potential deleterious mutations at a cost considerably less than de novo genome synthesis (supplementary text section B, "Time and cost"). In prior work, we used multiplex automated genome engineering [MAGE (*13*)] to remove all known UAG codons in groups of 10

[1]Department of Genetics, Harvard Medical School, Boston, MA 02115, USA. [2]Program in Chemical Biology, Harvard University, Cambridge, MA 02138, USA. [3]Department of Molecular, Cellular and Developmental Biology, Yale University, New Haven, CT 06520, USA. [4]Systems Biology Institute, Yale University, West Haven, CT 06516, USA. [5]Program in Medical Engineering and Medical Physics, Harvard–Massachusetts Institute of Technology (MIT) Division of Health Sciences and Technology, Cambridge, MA 02139, USA. [6]Department of Cellular and Molecular Physiology, Yale University, New Haven, CT 06520, USA. [7]Harvard College, Cambridge, MA 02138, USA. [8]Department of Systems Biology, Columbia University, College of Physicians and Surgeons, New York, NY 10032, USA. [9]MIT Lincoln Laboratory, Lexington, MA 02420, USA. [10]Department of Chemistry, The Scripps Research Institute, La Jolla, CA 92037, USA. [11]Center for Bits and Atoms, MIT, Cambridge, MA 02139, USA. [12]MIT Media Lab, MIT, Cambridge, MA 02139, USA. [13]Wyss Institute for Biologically Inspired Engineering, Harvard University, Boston, MA 02115, USA.

*Corresponding author. E-mail: farren.isaacs@yale.edu (F.J.I.); gchurch@genetics.med.harvard.edu (G.M.C.)

www.sciencemag.org/cgi/content/full/science.1242902/DC1

Supplementary Material for

Low Upper Limit to Methane Abundance on Mars

Christopher R. Webster,* Paul R. Mahaffy, Sushil K. Atreya, Gregory J. Flesch, Kenneth A. Farley, the MSL Science Team

*To whom correspondence should be addressed. E-mail: chris.r.webster@jpl.nasa.gov

Published 19 September 2013 on *Science* Express
DOI: 10.1126/science.1242902

This PDF file includes:

SUPPLEMENTAL INFORMATION:

Low Upper Limit to Methane Abundance on Mars

C. R. Webster, P. R. Mahaffy, S. K. Atreya, G. J. Flesch and K. A. Farley

The Tunable Laser Spectrometer (TLS) in the Sample Analysis at Mars (SAM) instrument suite on the Curiosity Rover

This instrument has been previously described in detail *(12, 13)*. Fig. S1 below emphasizes the optical layout for the methane measurement.

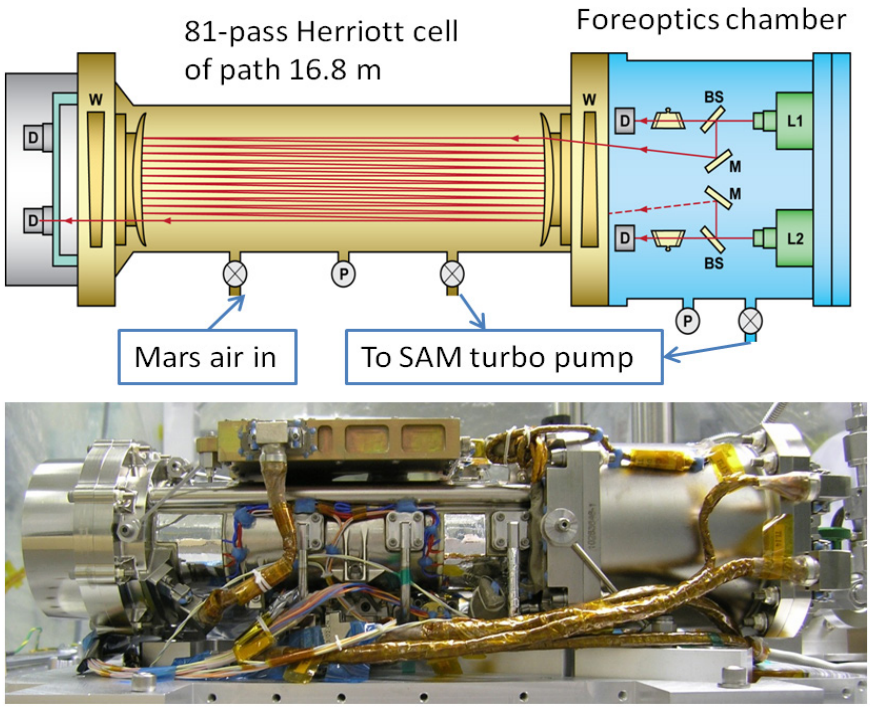

Figure S1. Top: Schematic of the TLS optical path. Prior to entering the 81-pass (16.8 m pathlength) sample cell through a wedged Ge window (W), the IC laser beam makes a single pass through ~9 cm of a foreoptics chamber containing lasers (L), beam-splitters (BS), reference gas cells (not used for methane measurement), and steering mirrors (M). Bottom: Photo of TLS flight spectrometer before integration into SAM with gold preamplifier on top of Herriott cell.

Methane spectroscopy and laser parameters:

The TLS interband cascade (IC) laser scans through a unique fingerprint of seven spectral lines in the υ_3 band: three $^{12}CH_4$ lines associated with R(3) and four subsequent $^{13}CH_4$ lines associated with R(3) transitions. Table S1 below lists the three $^{12}CH_4$ lines used for this study, as identified by both the HITRAN data base *(26)* and laboratory measurements. We create the labels e, f, g for these three lines, where the g line is strongest, and both e and f are about half the intensity of the g line.

Table S1. Spectral lines used to identify methane from HITRAN data base *(26)*

Spectral line center (cm^{-1})	Line-strength at 296 K (cm^{-1}/(molecule·cm^{-2}))	Ground-state energy (cm^{-1})	Assignment	Label
3057.687285	2.085E-19	62.8781	R(3)	g
3057.726529	1.245E-19	62.8768	R(3)	f
3057.760524	1.245E-19	62.8757	R(3)	e

The IC laser was developed at JPL, and operated near 245 K stabilized by a two-stage TEC cooler producing single-mode (>99%) continuous-wave output power with a linewidth retrieved from low-pressure (Doppler limited) spectra of ~10 MHz. This light was collimated using an efficient triple-lens collimator to produce ~1 mW laser power that passes through the foreoptics chamber then into the sample (Herriott) cell. Prior to entering the Herriott cell, the beam was attenuated by a factor of ~20 by a thin mylar sheet (not shown in Fig. S1) to reduce optical fringing and detector non-linearity. We note that the pre-launch settings for the TEC and laser current scans (used for calibration also) have not been changed and the target spectral line positions remain in our scan window. Very small (~linewidth) variations in the spectral line position are seen depending on the Curiosity heat ramp behavior, but we observe and track the methane lines continually for each spectrum through the simultaneously-recorded reference cell detector; the tracked methane spectrum arises from residual methane gas in the foreoptics chamber.

Evolved Gas Analysis Spectrum of Figure 1:

In Figure 1 we presented actual flight spectra downloaded from Curiosity rather than showing calculated HITRAN spectra. Spectra C and D are from the methane analysis presented here, but spectra A and B are from a different unrelated experiment on Mars in which a rock sample is heated (Evolved Gas Analysis (EGA) run) in a pyrolysis oven to produce evolved gas fed to TLS that was observed to contain methane. These spectra are shown here in part because they were taken AFTER the atmospheric methane runs and show that our CH_4 lines have not moved, and the instrument continues to work well with consistent capability to detect methane. The EGA spectra of Fig 1 (A, B) show the location of $^{12}CH_4$ and $^{13}CH_4$ lines in both the direct absorption and second harmonic (2f) spectrum.

Description of the Difference Method:

We determine Mars methane abundances by differencing full cell and empty cell results (not spectra), as described below. In a typical run on one sol, we collect (downlink) 26 empty cell spectra (2 minutes on board averaged each) followed by 26 full cell, then a few more empty for return-to-zero check. Cell temperatures and pressures are extremely stable during the complete sol run and contribute negligibly to our results (see later). We chose to record relatively long periods of continuous empty or full spectra to make sure that no drift (growth or loss) in retrieved methane abundance was observed during the run. We record sequential 2-minute empty cell spectra for ~1 hour followed by ~1 hour of sequential full cell spectra. We do not difference full-empty spectra before processing. Rather, with powerful computing resources now available, we process each of our 3 methane lines separately in each and all of our 2-minute spectra (by comparison with HITRAN calculations described below), then produce a combined efg-line average abundance for each spectrum that becomes a single raw 2-minute data point. Then, after applying common calibration factors and error contributions, we compare statistically the empty and full cell results for all the sols after normalizing to the empty cell mean values.

Direct and Second-harmonic (2f) Spectra

TLS is designed to simultaneously produce both direct absorption and second harmonic (2f) spectra, as is standard for commercial and laboratory tunable laser spectrometers *(27)*. Tunable laser spectrometers "scan" through spectral lines by applying a current ramp (usually saw-tooth) to the laser that through junction heating changes the wavelength by a small amount, the ramp repeated typically every one second (as done in TLS).

In direct absorption, absorption line depths that indicate gas abundance are measured as dips in the large light level on the detector as the laser is scanned. For very weak absorptions of ~1% or less (due to low gas amounts, too small path lengths or gas pressures, etc., and as expected for low methane (<20 ppbv) amounts) it is challenging for electronics and dynamic range to measure small changes in a large signal, and a "harmonic" detection is preferred. In harmonic detection, the very narrow laser linewidth (much narrower than the gas absorption line) is modulated ("dithered") at high frequency (say 10 kHz) by applying a sinusoidal component to the laser current ramp (increasing laser current is the normal method of tuning the laser across the spectral scan) with an amplitude that is small compared to the gas linewidth. So, if we modulate at 10 kHz and look at only the component of the detector signal at 10 kHz (using phase-sensitive detection), we would record a first-harmonic or first-derivative 1f spectrum as shown in Fig. S2. Outside the spectral line and at the line center, the laser is jiggling left and right where no difference exists, so it records zero in these places, but has its maximum signals (negative and positive) at the side of the line where the slope is maximum.

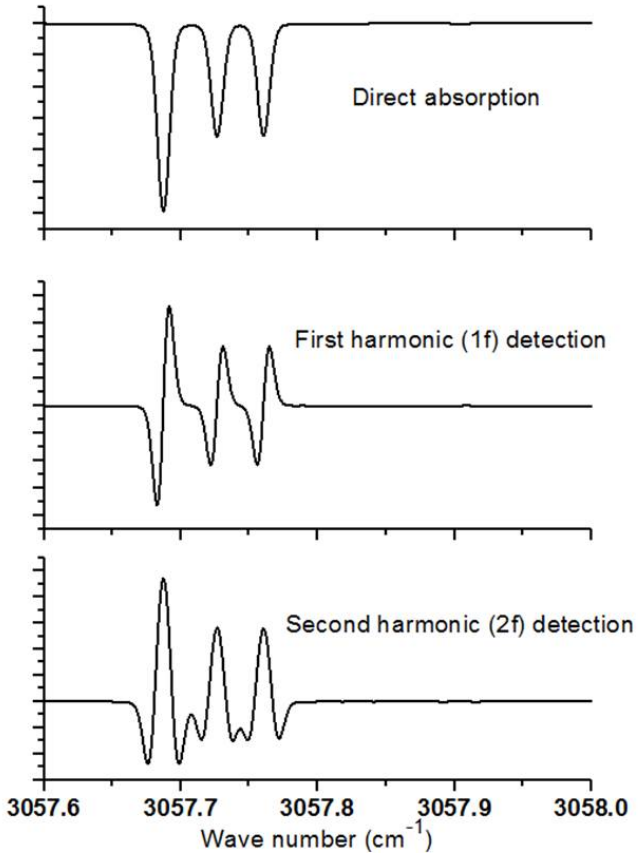

Figure S2. Comparison of theoretical line shapes of direct absorption, first harmonic (1f) detection and second harmonic (2f) detection.

If we now modulate at 10 kHz, but look at the component of the laser light on the detector that is at 20 kHz, we would record (as we do on TLS) the second-harmonic or second-derivative (2f) spectrum seen in Fig. S2. Both 1f and 2f spectral signals are zero-based in amplitude (electronics gain likes that) and move the detection frequency to higher frequency (kHz) compared to the direct (DC) spectrum, where 1/f noise is lower. Thus the harmonic method produces higher signal-to-noise spectra. The 1f spectrum is not usually used since it can have small vertical offsets and the line center position is a zero-crossing rather than a peak. The 2f spectrum is preferred since it has its peak in the same place as the direct absorption spectrum, and moves the detection regime to the higher (20 kHz) frequency.

Spectral Data Processing

The Beer-Lambert law models the optical transmission of light through an absorbing medium:

$$I_\nu = I_0 e^{-k(\nu)\rho l}$$

where I_ν is the transmitted light intensity at frequency ν, I_0 is the incident light intensity, $k(\nu)$ is a line shaping function that may be Doppler, Lorenzian, or Voigt, although the Doppler lineshape is a close approximation at Mars atmospheric pressures. ρ is the number density and l is the path length in cm. We use this model to determine the abundances of individual absorption lines present in our sampled measurements. The model needs many input spectral parameters for temperature dependence, air broadening, ground state energy, etc., and we use the HITRAN database for this information *(26)*. Direct absorption spectra produce good results for gases that have line center absorption depths of ~1% or greater. For higher sensitivity, we add a modulation to the laser current and then demodulate the returning detector signal at twice that frequency. This effectively gives us a second harmonic or *2f*

spectrum in which sensitivities of up to 2 parts in 10^5 are possible. See the section above and also Webster et al. *(27)* for a complete discussion.

Laser Power Normalization and Wave Number Scale

For a given channel (either CH_4 or CO_2/H_2O), TLS returns 3 spectra from the Herriott cell "science" detector, and 3 spectra from the reference channel detector. For both the Herriott cell and reference channel spectra, these 3 spectra are the direct absorption spectrum, the 2f spectrum, and a high-gain 2f spectrum. Our methane analysis is done using the 2f spectrum that is normalized to laser power from the direct absorption spectrum and mapped to a wave number scale using the reference detector signals. The high-gain 2f spectrum is not used since with only moderate gain increase (x16) it duplicates the 2f spectrum in signal-to-noise ratio but suffers from dynamic range restriction.

TLS also returns reference detector spectra recorded simultaneously with those from the science detector, and these are used to track the methane lines to provide the wave number scale for later processing. The methane signal (spectra) detected by the reference detector (located inside the foreoptics, as shown in Fig. S1) is due to residual methane in the foreoptics. The foreoptics contribution to the science spectrum is equivalent to about 90 ppbv for sols 79-292. The 2-stage thermoelectric cooler on the IC laser keeps the lines in the same position during the scans, with drifts in line positions over all sols of only about 1-2 linewidths that are tracked successfully.

For an amount of gas at a given pressure and temperature, the model will predict the depth and width (distribution in wave number) of the absorption by the gas sample for all sampled frequencies, allowing us to then compare our recorded spectra to the spectra produced by the model. But, in order to make this comparison, we must first normalize the recorded data. This process that takes level 0 data (spectra) and produces level 1 data (spectra) entails:

1. Removing a "null pulse" which is a measurement of the background light taken with the laser off, and recorded during every one second spectrum that is averaged on board for our 2-minute downlinked spectrum. This allows us to determine the direct absorption with respect to a percentage of transmitted light (i.e. 1% absorption: 99% transmission).
2. Removing any DC offsets in the harmonic spectra (described below).
3. Fit the baseline of the spectra. This sloping baseline results from the fact that the laser output power increases as it tunes through different wave numbers.
4. Assign a wave number (cm^{-1}) scale to the real spectra. We do this by using easily identifiable peaks of known wave number.

Once the raw spectra (level 0 data) are normalized (Fig. S3) as level 1 data, we can then use the HITRAN model to scale our real world data.

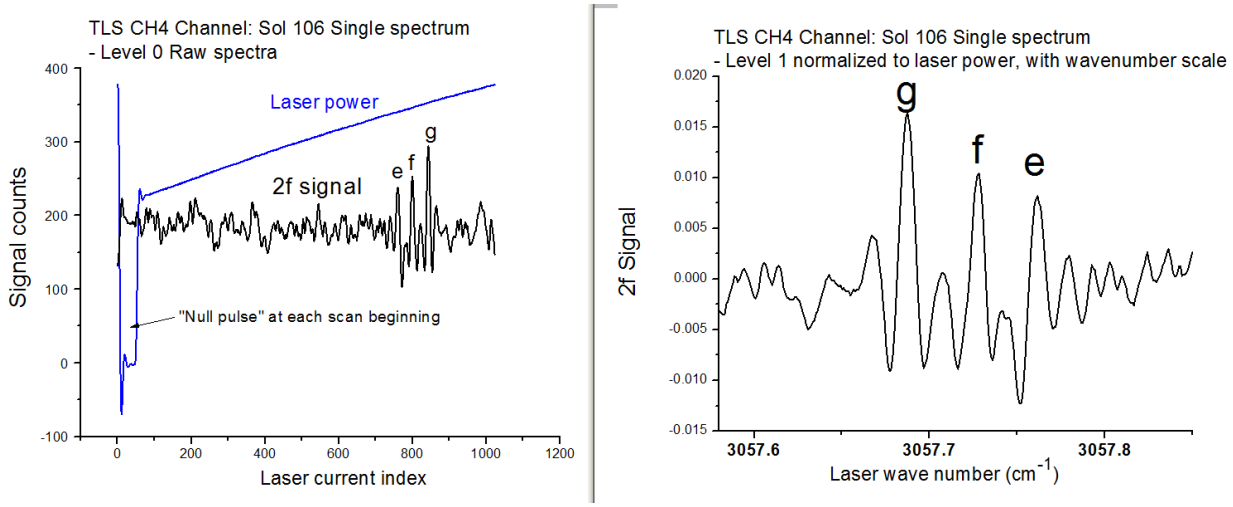

Fig. S3. Example of normalization of a real single spectrum (2 min.) downloaded for sol 106. The methane triplet lines e, f, g can be identified from Table S1 above. The left panel is the complete level 0 spectra, whereas the right panel that shows level 1 data (same 2-min. spectrum normalized to power and given wave number scale) has been

expanded in wave number to show the methane lines used and the occurrence of optical interference fringes that limit the detection method for a single 2-min. spectrum.

Producing Abundances
Using temperatures and pressures from our instrument for input, we iteratively run the model, varying the abundance in a converging algorithm until the synthetic spectra for the single line is the same size as our real spectrum (within some determined threshold). The convergence criteria are set to optimize for the 2f spectra.

For the methane analysis, we generate two results, one named "peak-to-peak" that returns the peak-to-peak signal amplitude (actually central peak to lobe-average) values, and a second named "integral" that returns the area of the 2f line between and above the bottom lobe minima positions (wave number). The peak-to-peak method finds the signal amplitude of the 2f maximum and lobe minima average, and is our preferred method since it produces somewhat lower scatter in our data, although results for either method are very close. The integral method, which is used for retrieving H, C, O isotope ratios *(19)* uses the following algorithm:

1. Find the global max of the 2f absorption spectra (peak)
2. Find the two local minima (2f lobes)
3. Fit a line between the two lobes
4. Using the lobes as integration boundaries, find the area between the fitted line and the spectra for both the direct and 2f spectra. Ratio this area between real and synthetic spectra and if ratio is outside the convergence threshold, iterate with new abundance.

Once the measurements converge, we ratio the resulting areas of the real spectra to the synthetic spectra which has a known abundance. For both methods, using the same laser modulation and gain throughout (pre-launch calibration and all Mars measurements), we relate the 2f signal size to the direct absorption size through calibration as described below, and like any flight project, we rigorously run our experiment as tested and calibrated pre-launch.

Calibration:
When analyzing direct absorption spectra with known pressure, temperature and pathlength, a Beer's law calculation using spectral line parameters from HITRAN can in theory provide the gas abundance without the need for calibration gases (i.e. someone else did the work when they created the data base). However, calibration gases serve the dual purpose of verifying the spectrometer response (a check of pathlength or number of passes in a cell, laser linewidth, pressure, mode purity, temperature, saturation, etc.) and also giving a direct calibration (relationship) between the direct absorption and the 2f channel with its various different gain stages.

The relative methane abundances reported here are calibrated using NIST-traceable methane in air provided by the NOAA-CMDL laboratory (provided by Jim Elkins group) specified to contain 88 ±0.5 ppbv. By injecting this gas into the TLS Herriott cell during pre-launch calibration runs of TLS and SAM in the NASA GSFC environmental chamber, we record both direct absorption and 2f signal sizes using the same conditions (e.g. laser scan, modulation, flight electronics and software, Herriott cell temperature and pressure, ramp heater) used on Mars. During the calibration run, the foreoptics is pumped out so that there is no contribution from foreoptics gas. The path length of the Herriott cell was verified to be 81 passes based on direct absorption measurements of these same methane lines using a second calibration cylinder (same provider) at 1800 ppbv. In addition, by adding pure methane gas at low pressures so that the lines are bleached to zero light transmission at line centers, the mode purity during the scan is verified. No change in alignment or detector signal sizes has been detected since pre-launch. Normalizing the mean value retrieved to 88 ppbv gives us a calibration result and uncertainty of 88.0 ±1.13 ppbv. We note that this absolute uncertainty of ±1.13 ppbv does not carry forward in our difference method described below, since it would only serve to change the mean value and upper limit slightly (by ~1 part in 88).

The foreoptics contribution to the difference method:
The difference method is described in the body of the main paper, and the sequence shown in Fig. S4 below. During the empty or full cell periods, the foreoptics and Herriott cell pressures are very stable; during a typical run (Sol 106) the temperatures and foreoptics pressure are stable to 0.02%, and the Herriott cell pressure during the full cell section is stable to 0.1%.

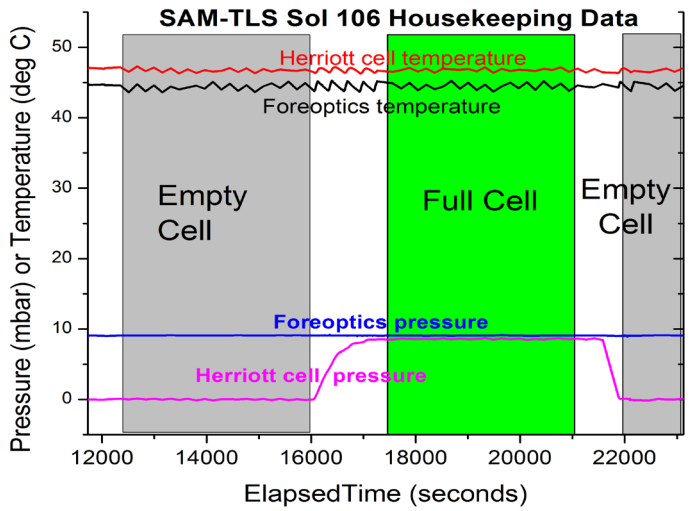

Figure S4. Housekeeping data from a single methane run (Sol 106) showing experiment sequence of 26 empty cell scans, 26 full cell scans, and 6 empty cell scans. Although the foreoptics pressure is different for some runs (see Tables 1 and S2), note that the foreoptics chamber pressure is constant during the empty and full Herriott cell runs on any given sol. For sols 306 and 313, the foreoptics pressure was first reduced to zero. The Herriott cell and foreoptics temperatures show the saw-tooth like effect of the small ramp applied to the heater to wash optical interference fringes.

Table S2. Ingest and foreoptics pressures.

Martian Sol after landing	Earth date	Ls (deg)	Gas ingest time and cell pressure (mbar)	Foreoptics pressure (mbar)
79	Oct 25th 2012	195.0	Night/8.0	11.5
81	Oct 27th 2012	196.2	Night/8.0	11.5
106	Nov 27th 2012	214.9	Night/8.5	10.9
292	June 1st 2013	328.6	Night/8.7	9.2
306	June 16th 2013	336.5	Day/8.1	~0
313	June 23rd 2013	340.5	Night/8.7	~0

During the long pre-launch and cruise phase to Mars, the foreoptics chamber leaked up to a significant pressure (~76 mbar) by the time we arrived at Mars. This pressure included terrestrial "Florida air" from the launch site that contained significant terrestrial methane gas (~10 ppmv) that showed up as a large methane signal (spectrum) on the Herriott cell science detector for both "empty" and "full" Herriott cell data, since the beam made one pass through the 9-cm length of the foreoptics. Moreover, our first attempts to measure methane on Mars showed methane spectra that increased in size with time during the empty and full cell scans that we attributed to diffusion (leakage) of the foreoptics methane gas into the Herriott cell during the run. Results from these runs made before sol 79 were discarded and not included in the analysis. To reduce the foreoptics contribution, we pumped down the foreoptics chamber in a series of steps for subsequent sol runs (80, 33, 11.5 mbar) until at 11.5 mbar we observed no detectable increase (or reduction) in the empty or full cell spectra with time over the run, so that we were confident that the leakage was negligible during the runs to follow. As a matter of good practice, for the last two data sets of sols 306 and 313, we further reduced the foreoptics pressure to close to zero by pumping on the chamber. As the data in Table S3 shows, the results for all 6 sols are consistent within measurement uncertainty. Note that the low foreoptics contribution in sols 306 and 313 reduces the scatter in the data somewhat, as shown in Table S3.

Because of the foreoptics contribution, all of our spectra (empty and full Herriott cell) look somewhat like those in Fig. S3 since (in the absence of significant Martian methane) they are dominated by the foreoptics contribution. We then process them as described above, and then look for differences in the empty and full cell results. Specifically, the "full" cell methane spectra are first processed as if the observed methane spectrum came only from the Herriott

cell, that is, we use the measured Herriott cell pressure and temperature to retrieve a "full cell" methane mixing ratio by comparison with HITRAN. Then for the "empty" cell spectra, we use the same mean temperatures and pressures of the full cell and process the empty cell spectra to reveal the "empty cell" methane mixing ratio. This method makes the difference method most sensitive to Herriott cell methane from Mars, should it be there. If there was no methane on Mars, the empty and full cell results would be identical. If there was 20 ppbv methane on Mars, the full cell result would be 20 ppbv larger than the empty cell result. For sols 79-292, for example, both the empty and full cell results are close to 90 ppbv, and for sols 306 and 313 it is <20 ppbv. For the difference data given in Table 1 and S1, the mean empty cell values for that specific run have been subtracted from the full cell values to provide the resulting Martian methane mixing ratio.

The inlet to the SAM-TLS instrument is a 3/16" internal diameter stainless steel tube heated to 50^{o}C containing a dust filter of sintered Inconel 0.5 micron particles that is located on the rover side ~1 m above the Martian surface, and was pointed at a variety of directions relative to the nominal wind direction.

Statistical analysis of data:
The spacecraft returns two-minute averaged signals for each of the three spectral absorption lines given in Table S1. The TLS measurements include methane absorption occurring both in the Herriott cell and along the optical path of the foreoptics prior to entry into the cell, as described in the main text. In our first four sol runs, the foreoptics region had terrestrial air with methane in it, allowing confident identification of the methane absorption lines and continuous monitoring of scan-to-scan line shifts. The foreoptics methane signal also introduces a substantial "blank" signal which must be removed to compute the amount of methane in the Mars atmosphere in the Herriott cell. For the later two sols 306 and 313, the foreoptics were pumped out before hand, and the measured background signals although much lower were treated in exactly the same way for all six sol data comparisons.

We treat each of these lines as a separate estimate of the absorption attributable to methane somewhere along the optic path. These absorptions were converted into an apparent methane mixing ratio in the Herriott cell by assuming that this is the only region in which methane occurs. As shown in Table S3, all of our sol runs except sol 306 were executed to produce 26 full cell points and 32 empty cell points. For sols 292 and 313 the heat ramp monitor showed that we had not quite reached temperature, and the first one and four points, respectively were removed from the analysis. For sol 306, the daytime run and rover power demand meant that the number of full, empty data points was limited to 22 and 18 points. No data points were removed from this analysis. Results for each of the six sol measurements (see Tables 1 and S3) show mean values ranging from -2.2 to 1.7 ppbv. In the absence of any notable difference in the atmospheric methane abundances retrieved on the six sols, we chose to merge the six individual data sets to obtain best estimates of the atmospheric methane amount, its uncertainty, and our upper limit methane value. We thus obtained 147 full cell points and 167 empty cell points that were then statistically analyzed as a single data set. For this calculation we subtracted the mean blank signal on each sol from the measured signals on that sol. The results are shown in Figure S5 as a histogram for the aggregated 6-sol data set. Each individual sol defines a broadly Gaussian distribution and all sols have statistically equivalent variance. These Gaussian distributions are also indicated in Figure S5. The mean empty cell value is by definition zero, while the blank-corrected full cell mean is 0.18 ± 0.67 ppbv. These data imply an upper limit with 95% confidence of 1.3 ppbv for the methane volume mixing ratio of the Martian atmosphere.

Table S3. Statistical data for each sol and 6-sol data treated as single data set.

Martian Sol after landing on Aug 6th 2012	Number of Full Cell points	Number of Empty Cell points	Mean CH4 value ± 1SEM (ppbv)
79	26	26	1.62 ± 2.03
81	26	32	1.71 ± 2.06
106	26	31	-0.55 ± 1.45
292	25	31	0.60 ± 1.74
306	22	18	-2.21 ± 0.94
313	22	27	-0.50 ± 0.94
All six sols treated as one data set	147	165	0.18 ± 0.67

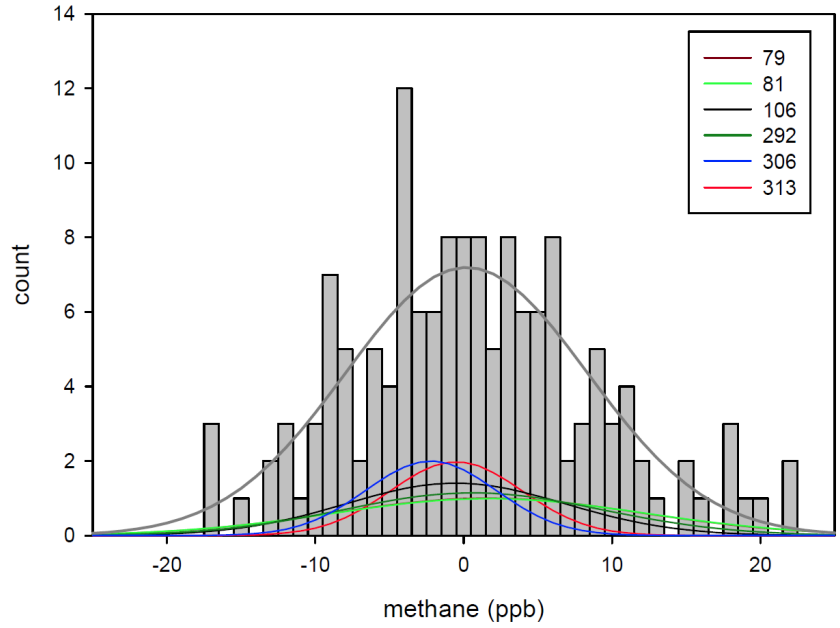

Figure S5. Histogram of data for full-empty cell differences from all data points from 6 sols (see text).

Mars Science Laboratory (MSL) Science Team

Aalto University
Osku Kemppinen

Applied Physics Laboratory (APL) at Johns Hopkins University
Nathan Bridges, Jeffrey R. Johnson, Michelle Minitti

Applied Research Associates, Inc. (ARA)
David Cremers

Arizona State University (ASU)
James F. Bell III, Lauren Edgar, Jack Farmer, Austin Godber, Meenakshi Wadhwa, Danika Wellington

Ashima Research
Ian McEwan, Claire Newman, Mark Richardson

ATOS Origin
Antoine Charpentier, Laurent Peret

Australian National University (ANU)
Penelope King

Bay Area Environmental Research Institute (BAER)
Jennifer Blank

Big Head Endian LLC
Gerald Weigle

Brock University
Mariek Schmidt

Brown University
Shuai Li, Ralph Milliken, Kevin Robertson, Vivian Sun

California Institute of Technology (Caltech)
Michael Baker, Christopher Edwards, Bethany Ehlmann, Kenneth Farley, Jennifer Griffes, John Grotzinger, Hayden Miller, Megan Newcombe, Cedric Pilorget, Melissa Rice, Kirsten Siebach, Katie Stack, Edward Stolper

Canadian Space Agency (CSA)
Claude Brunet, Victoria Hipkin, Richard Léveillé, Geneviève Marchand, Pablo Sobrón Sánchez

Capgemini France
Laurent Favot

Carnegie Institution of Washington
George Cody, Andrew Steele

Carnegie Mellon University
Lorenzo Flückiger, David Lees, Ara Nefian

Catholic University of America
Mildred Martin

Centre National de la Recherche Scientifique (CNRS)
Marc Gailhanou, Frances Westall, Guy Israël

Centre National d'Etudes Spatiales (CNES)
Christophe Agard, Julien Baroukh, Christophe Donny, Alain Gaboriaud, Philippe Guillemot, Vivian Lafaille, Eric Lorigny, Alexis Paillet, René Pérez, Muriel Saccoccio, Charles Yana

Centro de Astrobiología (CAB)
Carlos Armiens-Aparicio, Javier Caride Rodríguez, Isaías Carrasco Blázquez, Felipe Gómez Gómez , Javier Gómez-Elvira, Sebastian Hettrich, Alain Lepinette Malvitte, Mercedes Marín Jiménez, Jesús Martínez-Frías, Javier Martín-Soler, F. Javier Martín-Torres, Antonio Molina Jurado, Luis Mora-Sotomayor, Guillermo Muñoz Caro, Sara Navarro López, Verónica Peinado-González, Jorge Pla-García, José Antonio Rodriguez Manfredi, Julio José Romeral-Planelló, Sara Alejandra Sans Fuentes, Eduardo Sebastian Martinez, Josefina Torres Redondo, Roser Urqui-O'Callaghan, María-Paz Zorzano Mier

Chesapeake Energy
Steve Chipera

Commissariat à l'Énergie Atomique et aux Énergies Alternatives (CEA)
Jean-Luc Lacour, Patrick Mauchien, Jean-Baptiste Sirven

Concordia College
Heidi Manning

Cornell University
Alberto Fairén, Alexander Hayes, Jonathan Joseph, Steven Squyres, Robert Sullivan, Peter Thomas

CS Systemes d'Information
Audrey Dupont

Delaware State University
Angela Lundberg, Noureddine Melikechi, Alissa Mezzacappa

Denver Museum of Nature & Science
Julia DeMarines, David Grinspoon

Deutsches Zentrum für Luft- und Raumfahrt (DLR)
Günther Reitz

eINFORMe Inc. (at NASA GSFC)
Benito Prats

Finnish Meteorological Institute
Evgeny Atlaskin, Maria Genzer, Ari-Matti Harri, Harri Haukka, Henrik Kahanpää, Janne Kauhanen, Osku Kemppinen, Mark Paton, Jouni Polkko, Walter Schmidt, Tero Siili

GeoRessources
Cécile Fabre

Georgia Institute of Technology
James Wray, Mary Beth Wilhelm

Géosciences Environnement Toulouse (GET)
Franck Poitrasson

Global Science & Technology, Inc.
Kiran Patel

Honeybee Robotics
Stephen Gorevan, Stephen Indyk, Gale Paulsen

Imperial College
Sanjeev Gupta

Indiana University Bloomington
David Bish, Juergen Schieber

Institut d'Astrophysique Spatiale (IAS)
Brigitte Gondet, Yves Langevin

Institut de Chimie des Milieux et Matériaux de Poitiers (IC2MP)
Claude Geffroy

Institut de Recherche en Astrophysique et Planétologie (IRAP), Université de Toulouse
David Baratoux, Gilles Berger, Alain Cros, Claude d'Uston, Olivier Forni, Olivier Gasnault, Jérémie Lasue, Qiu-Mei Lee, Sylvestre Maurice, Pierre-Yves Meslin, Etienne Pallier, Yann Parot, Patrick Pinet, Susanne Schröder, Mike Toplis

Institut des Sciences de la Terre (ISTerre)
Éric Lewin

inXitu
Will Brunner

Jackson State University
Ezat Heydari

Jacobs Technology
Cherie Achilles, Dorothy Oehler, Brad Sutter

Laboratoire Atmosphères, Milieux, Observations Spatiales (LATMOS)
Michel Cabane, David Coscia, Guy Israël, Cyril Szopa

Laboratoire de Géologié de Lyon : Terre, Planète, Environnement (LGL-TPE)
Gilles Dromart

Laboratoire de Minéralogie et Cosmochimie du Muséum (LMCM)
François Robert, Violaine Sautter

Laboratoire de Planétologie et Géodynamique de Nantes (LPGN)
Stéphane Le Mouélic, Nicolas Mangold, Marion Nachon

Laboratoire Génie des Procédés et Matériaux (LGPM)
Arnaud Buch

Laboratoire Interuniversitaire des Systèmes Atmosphériques (LISA)
Fabien Stalport, Patrice Coll, Pascaline François, François Raulin, Samuel Teinturier

Lightstorm Entertainment Inc.
James Cameron

Los Alamos National Lab (LANL)
Sam Clegg, Agnès Cousin, Dorothea DeLapp, Robert Dingler, Ryan Steele Jackson, Stephen Johnstone, Nina Lanza, Cynthia Little, Tony Nelson, Roger C. Wiens, Richard B. Williams

Lunar and Planetary Institute (LPI)
Andrea Jones, Laurel Kirkland, Allan Treiman

Malin Space Science Systems (MSSS)
Burt Baker, Bruce Cantor, Michael Caplinger, Scott Davis, Brian Duston, Kenneth Edgett, Donald Fay, Craig Hardgrove, David Harker, Paul Herrera, Elsa Jensen, Megan R. Kennedy, Gillian Krezoski, Daniel Krysak, Leslie Lipkaman, Michael Malin, Elaina McCartney, Sean McNair, Brian Nixon, Liliya Posiolova, Michael Ravine, Andrew Salamon, Lee Saper, Kevin Stoiber, Kimberley Supulver, Jason Van Beek, Tessa Van Beek, Robert Zimdar

Massachusetts Institute of Technology (MIT)
Katherine Louise French, Karl Iagnemma, Kristen Miller, Roger Summons

Max Planck Institute for Solar System Research
Fred Goesmann, Walter Goetz, Stubbe Hviid

Microtel
Micah Johnson, Matthew Lefavor, Eric Lyness

Mount Holyoke College
Elly Breves, M. Darby Dyar, Caleb Fassett

NASA Ames
David F. Blake, Thomas Bristow, David DesMarais, Laurence Edwards, Robert Haberle, Tori Hoehler, Jeff Hollingsworth, Melinda Kahre, Leslie Keely, Christopher McKay, Mary Beth Wilhelm

NASA Goddard Space Flight Center (GSFC)
Lora Bleacher, William Brinckerhoff, David Choi, Pamela Conrad, Jason P. Dworkin, Jennifer Eigenbrode, Melissa Floyd, Caroline Freissinet, James Garvin, Daniel Glavin, Daniel Harpold, Andrea Jones, Paul Mahaffy, David K. Martin, Amy McAdam, Alexander Pavlov, Eric Raaen, Michael D. Smith, Jennifer Stern, Florence Tan, Melissa Trainer

NASA Headquarters
Michael Meyer, Arik Posner, Mary Voytek

NASA Jet Propulsion Laboratory (JPL)
Robert C, Anderson, Andrew Aubrey, Luther W. Beegle, Alberto Behar, Diana Blaney, David Brinza, Fred Calef, Lance Christensen, Joy A. Crisp, Lauren DeFlores, Bethany Ehlmann, Jason Feldman, Sabrina Feldman, Gregory Flesch, Joel Hurowitz, Insoo Jun, Didier Keymeulen, Justin Maki, Michael Mischna, John Michael Morookian, Timothy Parker, Betina Pavri, Marcel Schoppers, Aaron Sengstacken, John J. Simmonds, Nicole Spanovich, Manuel de la Torre Juarez, Ashwin R. Vasavada, Christopher R. Webster, Albert Yen
NASA Johnson Space Center (JSC)
Paul Douglas Archer, Francis Cucinotta, John H. Jones, Douglas Ming, Richard V. Morris, Paul Niles, Elizabeth Rampe

Nolan Engineering
Thomas Nolan

Oregon State University
Martin Fisk

Piezo Energy Technologies
Leon Radziemski

Planetary Science Institute

Bruce Barraclough, Steve Bender, Daniel Berman, Eldar Noe Dobrea, Robert Tokar, David Vaniman, Rebecca M. E. Williams, Aileen Yingst

Princeton University
Kevin Lewis

Rensselaer Polytechnic Institute (RPI)
Laurie Leshin

Retired
Timothy Cleghorn, Wesley Huntress, Gérard Manhès

Salish Kootenai College
Judy Hudgins, Timothy Olson, Noel Stewart

Search for Extraterrestrial Intelligence Institute (SETI I)
Philippe Sarrazin

Smithsonian Institution
John Grant, Edward Vicenzi, Sharon A. Wilson

Southwest Research Institute (SwRI)
Mark Bullock, Bent Ehresmann, Victoria Hamilton, Donald Hassler, Joseph Peterson, Scot Rafkin, Cary Zeitlin

Space Research Institute
Fedor Fedosov, Dmitry Golovin, Natalya Karpushkina, Alexander Kozyrev, Maxim Litvak, Alexey Malakhov, Igor Mitrofanov, Maxim Mokrousov, Sergey Nikiforov, Vasily Prokhorov, Anton Sanin, Vladislav Tretyakov, Alexey Varenikov, Andrey Vostrukhin, Ruslan Kuzmin

Space Science Institute (SSI)
Benton Clark, Michael Wolff

State University of New York (SUNY) Stony Brook
Scott McLennan

Swiss Space Office
Oliver Botta

TechSource
Darrell Drake

Texas A&M
Keri Bean, Mark Lemmon

The Open University
Susanne P. Schwenzer

United States Geological Survey (USGS) Flagstaff
Ryan B. Anderson, Kenneth Herkenhoff, Ella Mae Lee, Robert Sucharski

Universidad de Alcalá
Miguel Ángel de Pablo Hernández, Juan José Blanco Ávalos, Miguel Ramos

Universities Space Research Association (USRA)
Myung-Hee Kim, Charles Malespin, Ianik Plante

University College London (UCL)
Jan-Peter Muller

University Nacional Autónoma de México (UNAM)
Rafael Navarro-González

University of Alabama
Ryan Ewing

University of Arizona
William Boynton, Robert Downs, Mike Fitzgibbon, Karl Harshman, Shaunna Morrison

University of California Berkeley
William Dietrich, Onno Kortmann, Marisa Palucis

University of California Davis
Dawn Y. Sumner, Amy Williams

University of California San Diego
Günter Lugmair

University of California San Francisco
Michael A. Wilson

University of California Santa Cruz
David Rubin

University of Colorado Boulder
Bruce Jakosky

University of Copenhagen
Tonci Balic-Zunic, Jens Frydenvang, Jaqueline Kløvgaard Jensen, Kjartan Kinch, Asmus Koefoed, Morten Bo Madsen, Susan Louise Svane Stipp

University of Guelph
Nick Boyd, John L. Campbell, Ralf Gellert, Glynis Perrett, Irina Pradler, Scott VanBommel

University of Hawai'i at Manoa
Samantha Jacob, Tobias Owen, Scott Rowland

University of Helsinki
Evgeny Atlaskin, Hannu Savijärvi

University of Kiel
Eckart Boehm, Stephan Böttcher, Sönke Burmeister, Jingnan Guo, Jan Köhler, César Martín García, Reinhold Mueller-Mellin, Robert Wimmer-Schweingruber

University of Leicester
John C. Bridges

University of Maryland
Timothy McConnochie

University of Maryland Baltimore County
Mehdi Benna, Heather Franz

University of Maryland College Park
Hannah Bower, Anna Brunner

University of Massachusetts
Hannah Blau, Thomas Boucher, Marco Carmosino

University of Michigan Ann Arbor
Sushil Atreya, Harvey Elliott, Douglas Halleaux, Nilton Rennó, Michael Wong

University of Minnesota
Robert Pepin

University of New Brunswick
Beverley Elliott, John Spray, Lucy Thompson

University of New Mexico
Suzanne Gordon, Horton Newsom, Ann Ollila, Joshua Williams

University of Queensland
Paulo Vasconcelos

University of Saskatchewan
Jennifer Bentz

University of Southern California (USC)
Kenneth Nealson, Radu Popa

University of Tennessee Knoxville
Linda C. Kah, Jeffrey Moersch, Christopher Tate

University of Texas at Austin
Mackenzie Day, Gary Kocurek

University of Washington Seattle
Bernard Hallet, Ronald Sletten

University of Western Ontario
Raymond Francis, Emily McCullough

University of Winnipeg
Ed Cloutis

Utrecht University
Inge Loes ten Kate

Vernadsky Institute
Ruslan Kuzmin

Washington University in St. Louis (WUSTL)
Raymond Arvidson, Abigail Fraeman, Daniel Scholes, Susan Slavney, Thomas Stein, Jennifer Ward

Western University
Jeffrey Berger

York University
John E. Moores

References and Notes

1. S. K. Atreya, P. R. Mahaffy, H. B. Niemann, M. H. Wong, T. C. Owen, Composition and origin of the atmosphere of Jupiter—an update, and implications for the extrasolar giant planets. *Planet. Space Sci.* **51**, 105–112 (2003). doi:10.1016/S0032-0633(02)00144-7

2. H. A. Michelsen, G. L. Manney, C. R. Webster, R. D. May, M. R. Gunson, D. Baumgardner, K. K. Kelly, M. Loewenstein, J. R. Podolske, M. H. Proffitt, S. C. Wofsy, G. K. Yue, Intercomparison of ATMOS, SAGE II, and ER-2 observations in the Arctic vortex and extra-vortex air masses during spring 1993. *Geophys. Res. Lett.* **26**, 291–294 (1999). doi:10.1029/1998GL900282

3. V. A. Krasnopolsky, J. P. Maillard, T. C. Owen, Detection of methane in the martian atmosphere: evidence for life? *Icarus* **172**, 537–547 (2004). doi:10.1016/j.icarus.2004.07.004

4. V. Formisano, S. K. Atreya, T. Encrenaz, N. Ignatiev, M. Giuranna, Detection of methane in the atmosphere of Mars. *Science* **306**, 1758–1761 (2004). doi:10.1126/science.1101732 Medline

5. S. K. Atreya, P. R. Mahaffy, A. S. Wong, Methane and related trace species on Mars: Origin, loss, implications for life, and habitability. *Planet. Space Sci.* **55**, 358–369 (2007). doi:10.1016/j.pss.2006.02.005

6. A. Geminale, V. Formisano, G. Sindoni, Mapping methane in Martian atmosphere with PFS-MEX data. *Planet. Space Sci.* **59**, 137–148 (2011). doi:10.1016/j.pss.2010.07.011

7. M. J. Mumma, G. L. Villanueva, R. E. Novak, T. Hewagama, B. P. Bonev, M. A. Disanti, A. M. Mandell, M. D. Smith, Strong release of methane on Mars in northern summer 2003. *Science* **323**, 1041–1045 (2009). doi:10.1126/science.1165243 Medline

8. S. Fonti, G. A. Marzo, Mapping the methane on Mars. *Astron. Astrophys.* **512**, A51 (2010). doi:10.1051/0004-6361/200913178

9. V. A. Krasnopolsky, Search for methane and upper limits to ethane and SO_2 on Mars. *Icarus* **217**, 144–152 (2012). doi:10.1016/j.icarus.2011.10.019

10. G. L. Villanueva, M. J. Mumma, R. E. Novak, Y. L. Radeva, H. U. Käufl, A. Smette, A. Tokunaga, A. Khayat, T. Encrenaz, P. Hartogh, A sensitive search for Organics (CH_4, CH_3OH, H_2CO, C_2H_6, C_2H_2, C_2H_4), hydroperoxyl (HO2), nitrogen Compounds (N_2O, NH_3, HCN) and chlorine species (HCl, CH_3Cl) on Mars using ground-based high-resolution infrared spectroscopy. *Icarus* **223**, 11–27 (2013). doi:10.1016/j.icarus.2012.11.013

11. V. A. Krasnopolsky, A sensitive search for methane and ethane on Mars. *EPSC Abstracts* **6**, 49 (2011).

12. P. R. Mahaffy, C. R. Webster, M. Cabane, P. G. Conrad, P. Coll, S. K. Atreya, R. Arvey, M. Barciniak, M. Benna, L. Bleacher, W. B. Brinckerhoff, J. L. Eigenbrode, D. Carignan, M. Cascia, R. A. Chalmers, J. P. Dworkin, T. Errigo, P. Everson, H. Franz, R. Farley, S. Feng, G. Frazier, C. Freissinet, D. P. Glavin, D. N. Harpold, D. Hawk, V. Holmes, C. S. Johnson, A. Jones, P. Jordan, J. Kellogg, J. Lewis, E. Lyness, C. A. Malespin, D. K. Martin, J. Maurer, A. C. McAdam, D. McLennan, T. J. Nolan, M. Noriega, A. A. Pavlov,

B. Prats, E. Raaen, O. Sheinman, D. Sheppard, J. Smith, J. C. Stern, F. Tan, M. Trainer, D. W. Ming, R. V. Morris, J. Jones, C. Gundersen, A. Steele, J. Wray, O. Botta, L. A. Leshin, T. Owen, S. Battel, B. M. Jakosky, H. Manning, S. Squyres, R. Navarro-González, C. P. McKay, F. Raulin, R. Sternberg, A. Buch, P. Sorensen, R. Kline-Schoder, D. Coscia, C. Szopa, S. Teinturier, C. Baffes, J. Feldman, G. Flesch, S. Forouhar, R. Garcia, D. Keymeulen, S. Woodward, B. P. Block, K. Arnett, R. Miller, C. Edmonson, S. Gorevan, E. Mumm, The Sample Analysis at Mars Investigation and Instrument Suite. *Space Sci. Rev.* **170**, 401–478 (2012). doi:10.1007/s11214-012-9879-z

13. C. R. Webster, P. R. Mahaffy, G. J. Flesch, P. B. Niles, J. H. Jones, L. A. Leshin, S. K. Atreya, J. C. Stern, L. E. Christensen, T. Owen, H. Franz, R. O. Pepin, A. Steele, C. Achilles, C. Agard, J. A. Alves Verdasca, R. Anderson, R. Anderson, D. Archer, C. Armiens-Aparicio, R. Arvidson, E. Atlaskin, A. Aubrey, B. Baker, M. Baker, T. Balic-Zunic, D. Baratoux, J. Baroukh, B. Barraclough, K. Bean, L. Beegle, A. Behar, J. Bell, S. Bender, M. Benna, J. Bentz, G. Berger, J. Berger, D. Berman, D. Bish, D. F. Blake, J. J. Blanco Avalos, D. Blaney, J. Blank, H. Blau, L. Bleacher, E. Boehm, O. Botta, S. Böttcher, T. Boucher, H. Bower, N. Boyd, B. Boynton, E. Breves, J. Bridges, N. Bridges, W. Brinckerhoff, D. Brinza, T. Bristow, C. Brunet, A. Brunner, W. Brunner, A. Buch, M. Bullock, S. Burmeister, M. Cabane, F. Calef, J. Cameron, J. Campbell, B. Cantor, M. Caplinger, J. Caride Rodríguez, M. Carmosino, I. Carrasco Blázquez, A. Charpentier, S. Chipera, D. Choi, B. Clark, S. Clegg, T. Cleghorn, E. Cloutis, G. Cody, P. Coll, P. Conrad, D. Coscia, A. Cousin, D. Cremers, J. Crisp, A. Cros, F. Cucinotta, C. d'Uston, S. Davis, M. Day, M. de la Torre Juarez, L. DeFlores, D. DeLapp, J. DeMarines, D. DesMarais, W. Dietrich, R. Dingler, C. Donny, B. Downs, D. Drake, G. Dromart, A. Dupont, B. Duston, J. Dworkin, M. D. Dyar, L. Edgar, K. Edgett, C. Edwards, L. Edwards, B. Ehlmann, B. Ehresmann, J. Eigenbrode, B. Elliott, H. Elliott, R. Ewing, C. Fabre, A. Fairén, K. Farley, J. Farmer, C. Fassett, L. Favot, D. Fay, F. Fedosov, J. Feldman, S. Feldman, M. Fisk, M. Fitzgibbon, M. Floyd, L. Flückiger, O. Forni, A. Fraeman, R. Francis, P. François, C. Freissinet, K. L. French, J. Frydenvang, A. Gaboriaud, M. Gailhanou, J. Garvin, O. Gasnault, C. Geffroy, R. Gellert, M. Genzer, D. Glavin, A. Godber, F. Goesmann, W. Goetz, D. Golovin, F. Gómez Gómez, J. Gómez-Elvira, B. Gondet, S. Gordon, S. Gorevan, J. Grant, J. Griffes, D. Grinspoon, J. Grotzinger, P. Guillemot, J. Guo, S. Gupta, S. Guzewich, R. Haberle, D. Halleaux, B. Hallet, V. Hamilton, C. Hardgrove, D. Harker, D. Harpold, A. M. Harri, K. Harshman, D. Hassler, H. Haukka, A. Hayes, K. Herkenhoff, P. Herrera, S. Hettrich, E. Heydari, V. Hipkin, T. Hoehler, J. Hollingsworth, J. Hudgins, W. Huntress, J. Hurowitz, S. Hviid, K. Iagnemma, S. Indyk, G. Israël, R. Jackson, S. Jacob, B. Jakosky, E. Jensen, J. K. Jensen, J. Johnson, M. Johnson, S. Johnstone, A. Jones, J. Joseph, I. Jun, L. Kah, H. Kahanpää, M. Kahre, N. Karpushkina, W. Kasprzak, J. Kauhanen, L. Keely, O. Kemppinen, D. Keymeulen, M. H. Kim, K. Kinch, P. King, L. Kirkland, G. Kocurek, A. Koefoed, J. Köhler, O. Kortmann, A. Kozyrev, J. Krezoski, D. Krysak, R. Kuzmin, J. L. Lacour, V. Lafaille, Y. Langevin, N. Lanza, J. Lasue, S. Le Mouélic, E. M. Lee, Q. M. Lee, D. Lees, M. Lefavor, M. Lemmon, A. Lepinette Malvitte, R. Léveillé, É. Lewin-Carpintier, K. Lewis, S. Li, L. Lipkaman, C. Little, M. Litvak, E. Lorigny, G. Lugmair, A. Lundberg, E. Lyness, M. Madsen, J. Maki, A. Malakhov, C. Malespin, M. Malin, N. Mangold, G. Manhes, H. Manning, G. Marchand, M. Marín Jiménez, C. Martín García, D. Martin, M. Martin, J. Martínez-Frías, J. Martín-Soler, F. J. Martín-Torres, P. Mauchien, S. Maurice,

A. McAdam, E. McCartney, T. McConnochie, E. McCullough, I. McEwan, C. McKay, S. McLennan, S. McNair, N. Melikechi, P. Y. Meslin, M. Meyer, A. Mezzacappa, H. Miller, K. Miller, R. Milliken, D. Ming, M. Minitti, M. Mischna, I. Mitrofanov, J. Moersch, M. Mokrousov, A. Molina Jurado, J. Moores, L. Mora-Sotomayor, J. M. Morookian, R. Morris, S. Morrison, R. Mueller-Mellin, J. P. Muller, G. Muñoz Caro, M. Nachon, S. Navarro López, R. Navarro-González, K. Nealson, A. Nefian, T. Nelson, M. Newcombe, C. Newman, H. Newsom, S. Nikiforov, B. Nixon, E. Noe Dobrea, T. Nolan, D. Oehler, A. Ollila, T. Olson, M. Á. de Pablo Hernández, A. Paillet, E. Pallier, M. Palucis, T. Parker, Y. Parot, K. Patel, M. Paton, G. Paulsen, A. Pavlov, B. Pavri, V. Peinado-González, L. Peret, R. Perez, G. Perrett, J. Peterson, C. Pilorget, P. Pinet, J. Pla-García, I. Plante, F. Poitrasson, J. Polkko, R. Popa, L. Posiolova, A. Posner, I. Pradler, B. Prats, V. Prokhorov, S. W. Purdy, E. Raaen, L. Radziemski, S. Rafkin, M. Ramos, E. Rampe, F. Raulin, M. Ravine, G. Reitz, N. Rennó, M. Rice, M. Richardson, F. Robert, K. Robertson, J. A. Rodriguez Manfredi, J. J. Romeral-Planelló, S. Rowland, D. Rubin, M. Saccoccio, A. Salamon, J. Sandoval, A. Sanin, S. A. Sans Fuentes, L. Saper, P. Sarrazin, V. Sautter, H. Savijärvi, J. Schieber, M. Schmidt, W. Schmidt, D. Scholes, M. Schoppers, S. Schröder, S. Schwenzer, E. Sebastian Martinez, A. Sengstacken, R. Shterts, K. Siebach, T. Siili, J. Simmonds, J. B. Sirven, S. Slavney, R. Sletten, M. Smith, P. Sobrón Sánchez, N. Spanovich, J. Spray, S. Squyres, K. Stack, F. Stalport, T. Stein, N. Stewart, S. L. Stipp, K. Stoiber, E. Stolper, B. Sucharski, R. Sullivan, R. Summons, D. Sumner, V. Sun, K. Supulver, B. Sutter, C. Szopa, F. Tan, C. Tate, S. Teinturier, I. ten Kate, P. Thomas, L. Thompson, R. Tokar, M. Toplis, J. Torres Redondo, M. Trainer, A. Treiman, V. Tretyakov, R. Urqui-O'Callaghan, J. Van Beek, T. Van Beek, S. VanBommel, D. Vaniman, A. Varenikov, A. Vasavada, P. Vasconcelos, E. Vicenzi, A. Vostrukhin, M. Voytek, M. Wadhwa, J. Ward, E. Weigle, D. Wellington, F. Westall, R. C. Wiens, M. B. Wilhelm, A. Williams, J. Williams, R. Williams, R. B. Williams, M. Wilson, R. Wimmer-Schweingruber, M. Wolff, M. Wong, J. Wray, M. Wu, C. Yana, A. Yen, A. Yingst, C. Zeitlin, R. Zimdar, M. P. Zorzano Mier; MSL Science Team, Isotope ratios of H, C, and O in CO_2 and H_2O of the martian atmosphere. *Science* **341**, 260–263 (2013). doi:10.1126/science.1237961 Medline

14. Materials and methods are available as supplementary materials on *Science* Online.

15. F. Lefèvre, F. Forget, Observed variations of methane on Mars unexplained by known atmospheric chemistry and physics. *Nature* **460**, 720–723 (2009). doi:10.1038/nature08228 Medline

16. A. S. Wong, S. K. Atreya, T. Encrenaz, Chemical markers of possible hot spots on Mars. *J. Geophys. Res.* **108**, (E4), 5026 (2003). doi:10.1029/2002JE002003

17. K. J. Zahnle, R. S. Freedman, D. C. Catling, Is there methane on Mars? *Icarus* **212**, 493–503 (2011). doi:10.1016/j.icarus.2010.11.027

18. R. A. Kerr, Planetary science. Question of martian methane is still up in the air. *Science* **338**, 733 (2012). doi:10.1126/science.338.6108.733 Medline

19. V. A. Krasnopolsky, Some problems related to the origin of methane on Mars. *Icarus* **180**, 359–367 (2006). doi:10.1016/j.icarus.2005.10.015

20. P. R. Christensen, Mars as seen from the 2001 Mars Odyssey Thermal Emission Imaging System experiment. *EOS Trans. AGU Fall Meet. Suppl.* **84** (46), Abstract P21A-02, 2003.

21. T. Encrenaz, T. K. Greathouse, M. J. Richter, J. H. Lacy, T. Fouchet, B. Bézard, F. Lefèvre, F. Forget, S. K. Atreya, A stringent upper limit to SO_2 in the Martian atmosphere. *Astron. Astrophys.* **530**, 1–5 (2011). doi:10.1051/0004-6361/201116820

22. S. K. Atreya, O. Witasse, V. F. Chevrier, F. Forget, P. R. Mahaffy, P. Buford Price, C. R. Webster, R. W. Zurek, Methane on Mars: Current observations, interpretation, and future plans. *Planet. Space Sci.* **59**, 133–136 (2011). doi:10.1016/j.pss.2010.10.008

23. S. K. Atreya, A. S. Wong, N. O. Renno, W. M. Farrell, G. T. Delory, D. D. Sentman, S. A. Cummer, J. R. Marshall, S. C. Rafkin, D. C. Catling, Oxidant enhancement in martian dust devils and storms: implications for life and habitability. *Astrobiology* **6**, 439–450 (2006). doi:10.1089/ast.2006.6.439 Medline

24. G. T. Delory, W. M. Farrell, S. K. Atreya, N. O. Renno, A. S. Wong, S. A. Cummer, D. D. Sentman, J. R. Marshall, S. C. Rafkin, D. C. Catling, Oxidant enhancement in martian dust devils and storms: storm electric fields and electron dissociative attachment. *Astrobiology* **6**, 451–462 (2006). doi:10.1089/ast.2006.6.451 Medline

25. W. M. Farrell, G. T. Delory, S. K. Atreya, Martian Dust Storms as a Possible Sink of Atmospheric Methane. *J. Geophys. Res.* **33**, (2006). 10.1029/2006GL027210

26. L. S. Rothman, I. E. Gordon, A. Barbe, D. C. Benner, P. F. Bernath, M. Birk, V. Boudon, L. R. Brown, A. Campargue, J.-P. Champion, K. Chance, L. H. Coudert, V. Dana, V. M. Devi, S. Fally, J.-M. Flaud, R. R. Gamache, A. Goldman, D. Jacquemart, I. Kleiner, N. Lacome, W. J. Lafferty, J.-Y. Mandin, S. T. Massie, S. N. Mikhailenko, C. E. Miller, N. Moazzen-Ahmadi, O. V. Naumenko, A. V. Nikitin, J. Orphal, V. I. Perevalov, A. Perrin, A. Predoi-Cross, C. P. Rinsland, M. Rotger, M. Šimečková, M. A. H. Smith, K. Sung, S. A. Tashkun, J. Tennyson, R. A. Toth, A. C. Vandaele, J. Vander Auwera, The HITRAN 2008 Molecular Spectroscopic Database. *J. Quant. Spectrosc. Radiat. Transf.* **110**, 533–572 (2009). doi:10.1016/j.jqsrt.2009.02.013

27. C. R. Webster, R. T. Menzies, E. D. Hinkley, "Infrared laser absorption: theory and applications," *Laser Remote Chemical Analysis*, R.M. Measures, ed., Wiley, New York, Chap. 3, (1988).